Journal of Computational Acoustics, Vol. 4, No. 3 (1996) 291–319

A NUMERICAL STUDY OF NONLINEAR PROPAGATION OF DISTURBANCES IN TWO-DIMENSIONS

TONY W. H. SHEU* and C. C. FANG†
Department of Naval Architecture and Ocean Engineering,
National Taiwan University, 73 Chou-Shan Rd., Taipei, Taiwan, Republic of China

Received 23 February 1995
Revised 8 November 1995

In the spirit of the method of characteristics, we present in this paper a generalized Taylor-Galerkin finite element model to simulate the nonlinear propagation of finite-amplitude disturbances. In a nonlinear Euler system, the multi-dimensional formulation is constructed through the conservation variables. Noticeable is that the scheme is found to exhibit high-phase-accuracy, together with minimal numerical damping. This scheme, therefore, is best-suited to simulation of disturbances in an acoustic field. To begin with, we validate the characteristic model by simulating two transport problems amenable to analytic solutions. Motivated by the apparent success, we apply the proposed third-order accurate upwind model to investigate a truly nonlinear acoustic field. The present analysis is intended to elucidate to what extent the nondissipative, nondispersive and isotropic characteristics pertaining to three wave modes of the acoustic system are still valid.

1. Introduction

The phenomena associated with acoustic propagation can be well described by a set of linearized hyperbolic Euler differential equations. It has been among the subjects of interest to scientists for years and is of practical relevance to human beings on a daily basis. Considerable effort has been directed toward the theoretical and experimental analyses after the emergence of a theory of sound propagation. Much of the work in this area has been carried out by scientists who have mainly considered the propagation of small-amplitude disturbances in a linearized Euler system. For situations where disturbances are of finite amplitudes, acoustics certainly turn out to be fluid dynamics so that a linear analysis becomes inadequate, and the nonlinear phenomena must be taken into account.[1] These nonlinearities make the Euler system hardly amenable to analytical solutions. As a consequence, researchers in industrial circles or academic institutes have been motivated to search for an alternative to the experimental calibration. Thanks to ever-improving computer hardware and ever-refining hyperbolic theory,[2,3] the technique of numerical simulation has reached maturity nowadays and has been regarded as a complementary tool for analyses of flow conditions hitherto inaccessible.

*Professor, FAX: 886-2-3929885; E-mail: sheu@indy.na.ntu.edu.tw.
†Ph. D candidate.

The hyperbolic partial differential equation was first attempted numerically by Lax,[4] followed by MacCormack *et al.* The readers are referred to the recent review article for additional details.[5] Apart from the embedded characteristics, it is of particular importance to preserve the dispersion relation for analyses in association with acoustic computations so as to accurately model its wave motion. In this regard, it is plausible to apply a high-order upwind scheme to predict the evolution of disturbances. Moreover, it is hoped that the developed computer code is applicable to acoustic computations in the domain of an arbitrary shape. To achieve this goal we formulate the numerical model underlying the framework of Taylor-Galerkin finite element method.

An outline of the remainder of the paper follows: In Sec. 2, we describe the mathematic models applicable to acoustic and nonlinear fluid dynamic systems. Three basic waves that are supported by the linearized Euler system are also briefly recalled. Section 3 is devoted to the Taylor-Galerkin finite element model. Phase response and the modified equation analyses form the main theme of this section. Two test problems amenable to analytic solutions are presented in Sec. 4 corroborate the theoretical analyses. Finally, in Sec. 5 we use the proposed characteristic model extended here to the transport of two-dimensional disturbances of different amplitudes. We address the importance of nonlinearities and provide answers how wave profiles with larger amplitudes deviate with those underlying the linear theory.

2. Mathematical Model

2.1. *Linearized Euler equations for acoustic disturbances*

Acoustics are governed by the linearized Euler equations. As is usual, both velocities u, v and thermodynamic properties p, ρ, are decomposed into mean and fluctuating parts. Hereinafter, we denote the fluctuating quantities as those with the superscript "$\prime$"; while the mean field variables with the subscript "0". The propagation of fluctuating disturbances, namely (ρ', u', v', p'), in a mean flow of uniform density ρ_0, pressure p_0 and velocity u_0 consequently relies on the following dimensional system in two dimensions:

$$\frac{\partial \mathbf{U}}{\partial t} + \frac{\partial \mathbf{F}}{\partial x} + \frac{\partial \mathbf{G}}{\partial y} = \mathbf{Q}, \tag{2.1}$$

where

$$\mathbf{U} = (\rho', u', v', p')^{\mathrm{T}}, \tag{2.2}$$

$$\mathbf{F} = (\rho_0 u' + \rho' u_0, u_0 u' + p'/\rho_0, u_0 v', u_0 p' + k p_0 u')^{\mathrm{T}}, \tag{2.3}$$

$$\mathbf{G} = (\rho_0 v', 0, p'/\rho_0, k p_0 v')^{\mathrm{T}}. \tag{2.4}$$

In (2.2)–(2.4), the superscript T represents the transpose notation. As to k appearing in (2.3) and (2.4), it denotes the specific heat ratio of the working media. On the right hand side of (2.1), $\mathbf{Q}$ stands for the distributed unsteady sources. Under these circumstances, this linearized hyperbolic system can support acoustic, entropy, and vorticity wave modes.

Any outgoing disturbance, in theory, is the result of the nondispersive, nondissipative, and isotropic propagation characteristics. We considered acoustic, vorticity, and the entropy waves in an environment characterized as having constant velocity u_0 and sound speed a_0. These linearized hyperbolic equations (2.1)–(2.4) are made dimensionless and are amenable to exact solutions, as given by Tam and Webb.[6] Six reference quantities are involved, namely the length scale $\Delta x(\equiv \Delta y)$, velocity scale a_0, time scale $\Delta x/a_0$, density scale ρ_0, pressure scale $\rho_0 a_0^2$, and the specific total energy scale a_0^2. The resulting dimensionless equations are furthermore transformed to a coordinate system moving along with the mean flow.

Entropy waves are nondispersive, nondissipative but highly directional. They propagate, with the speed of particle flow, along the direction of the mean flow. The test case considered here is mainly intended to identify the importance of the nonlinear effect in the Euler system.

The entropy wave consists of density fluctuations alone, given by the Gaussian profile. The initial distributions of the investigated disturbance are given by

$$p' = u' = v' = 0\,, \tag{2.5}$$

$$\rho' = \varepsilon_e \exp\left(-\frac{\ln 2}{25}(x^2 + y^2)\right)\,, \tag{2.6}$$

where ε_e denotes the entropy pulse amplitude. According to the work of Tam and Webb,[6] the analytic solutions for (2.1), subject to the initial conditions (2.5)–(2.6), take the following form:

$$p' = u' = v' = 0\,, \tag{2.7}$$

$$\rho' = \varepsilon_e \exp\left(-\frac{\ln 2}{25}((x - mt)^2 + y^2)\right)\,, \tag{2.8}$$

where $m = \frac{u_0}{a_0}$ is the mean flow Mach number. This amounts to implying that the entropy wave is convected downstream by the uniform flow without being distorted.

Vorticity waves are also classified as being nondispersive and nondissipative. This class of waves consists of fluctuated velocities propagating solely along the mean flow direction. No pressure or density fluctuation is involved in this wave mode. Initially, we considered fluctuations given by

$$\rho' = p' = 0\,, \tag{2.9}$$

$$u' = \varepsilon_v y \exp\left(-\frac{\ln 2}{25}(x^2 + y^2)\right)\,, \tag{2.10}$$

$$v' = -\varepsilon_v x \exp\left(-\frac{\ln 2}{25}(x^2 + y^2)\right)\,, \tag{2.11}$$

where ε_v stands for the vorticity pulse amplitude. Of importance is that the vorticity wave possesses the same propagation characteristics as those of the entropy wave since they accommodate the same dispersion relation. The analytic solutions for the linearized

Euler system, together with the initial fluctuations given by (2.9)–(2.11), take the following form:[6]

$$p' = \rho' = 0\,, \tag{2.12}$$

$$u' = \varepsilon_v y \exp\left(-\frac{\ln 2}{25}((x-mt)^2 + y^2)\right)\,, \tag{2.13}$$

$$v' = -\varepsilon_v (x-mt) \exp\left(-\frac{\ln 2}{25}((x-mt)^2 + y^2)\right)\,. \tag{2.14}$$

Acoustic waves are isotropic, nondispersive, nondissipative and propagate with the speed of sound. Initially, the fluctuations take the following form:

$$u' = v' = 0\,, \tag{2.15}$$

$$p' = \rho' = \varepsilon_a \exp\left(-\frac{\ln 2}{9}(x^2 + y^2)\right)\,, \tag{2.16}$$

where ε_a represents the pressure pulse amplitude. The analytical solutions associated with the above initial fluctuations are given by[6]

$$u'(x, y, t) = \frac{\varepsilon_a (x-mt)}{2k\dfrac{\ln 2}{9}\sqrt{(x-mt)^2 + y^2}} \times \int_0^\infty \zeta \exp\left(-\frac{\zeta^2}{4\dfrac{\ln 2}{9}}\right) \sin(\zeta t) J_1(\zeta\sqrt{(x-mt)^2 + y^2}) d\zeta\,, \tag{2.17}$$

$$v'(x, y, t) = \frac{\varepsilon_a y}{2k\dfrac{\ln 2}{9}\sqrt{(x-mt)^2 + y^2}} \times \int_0^\infty \zeta \exp\left(-\frac{\zeta^2}{4\dfrac{\ln 2}{9}}\right) \sin(\zeta t) J_1(\zeta\sqrt{(x-mt)^2 + y^2}) d\zeta\,, \tag{2.18}$$

$$p'(x, y, t) = \rho'(x, y, t) = \frac{\varepsilon_a}{2\dfrac{\ln 2}{9}} \int_0^\infty \zeta \exp\left(-\frac{\zeta^2}{4\dfrac{\ln 2}{9}}\right) \cos(\zeta t) J_0(\zeta\sqrt{(x-mt)^2 + y^2}) d\zeta\,, \tag{2.19}$$

where J_1 and J_0 stand for the Bessel function of order 1 and 0, respectively.

2.2. *Nonlinear acoustic system*

Consider an arbitrary disturbance of small amplitude which is superimposed on a quiescent mean flow field. The investigated Euler equations capable of describing the propagation of disturbances (ρ', u', v', e') are given by

$$\mathbf{U}_t + \mathbf{F}_x + \mathbf{G}_y = \mathbf{Q}\,, \tag{2.20}$$

where

$$\mathbf{U} = (\rho,\ \rho u',\ \rho v',\ \rho e')^{\mathrm{T}}\,, \tag{2.21}$$

$$\mathbf{F} = (\rho u',\ \rho u'^2 + p',\ \rho u'v',\ u'(p' + \rho e'))^{\mathrm{T}}\,, \tag{2.22}$$

$$\mathbf{G} = (\rho v',\ \rho u'v',\ \rho v'^2 + p',\ v'(p' + \rho e'))^{\mathrm{T}}\,, \tag{2.23}$$

$$\mathbf{Q} = (0,\ 0,\ 0,\ -p_0 u'_x - p_0 v'_y)^{\mathrm{T}}\,. \tag{2.24}$$

To close the above hyperbolic system, we adopt the following constitutive equation:

$$p' = (k-1)\rho\left(e' - \frac{1}{2}(u'^2 + v'^2)\right) - p_0 + (k-1)e_0(\rho_0 + \rho')\,, \tag{2.25}$$

where $e_0 = e - e'$ is the specific mean total energy. For an initially quiescent flow, the thermodynamic properties follow the following relationship:

$$e_0 = \frac{1}{k-1}\frac{p_0}{\rho_0} \quad \left(\text{or } e = \frac{1}{k-1}\frac{p}{\rho} + \frac{1}{2}(u^2 + v^2)\right)\,. \tag{2.26}$$

Under these circumstances, the source vector becomes $\mathbf{Q} = (0,\ 0,\ 0,\ -p_0(u'_x + v'_y))$. Together with the initial conditions and the above equation of state, we are led to

$$p' = (k-1)\rho\left(e' - \frac{1}{2}(u'^2 + v'^2)\right) + \frac{p_0}{\rho_0}\rho'\,. \tag{2.27}$$

To summarize, the investigated hyperbolic system for modeling the transport of disturbances takes the following form:

$$\frac{\partial}{\partial t}\begin{pmatrix}\rho\\ \rho u'\\ \rho v'\\ \rho e'\end{pmatrix} + \frac{\partial}{\partial x}\begin{pmatrix}\rho u'\\ \rho u'^2 + p'\\ \rho u'v'\\ u'(p' + \rho e')\end{pmatrix} + \frac{\partial}{\partial y}\begin{pmatrix}\rho v'\\ \rho u'v'\\ \rho v'^2 + p'\\ v'(p' + \rho e')\end{pmatrix} = \begin{pmatrix}0\\ 0\\ 0\\ -p_0 u'_x - p_0 v'_y\end{pmatrix}\,. \tag{2.28}$$

Initial conditions considered comprise three sets of fluctuations. The first set of disturbances concerns the following initial condition:

$$\mathbf{U}_1(t=0) = \begin{pmatrix}\rho_0 + \varepsilon_e \exp\left(-\dfrac{\ln 2}{25}(x^2 + y^2)\right)\\ 0\\ 0\\ 0\end{pmatrix}\,, \tag{2.29}$$

or

$$p' = u' = v' = 0\,, \tag{2.30}$$

$$\rho' = \varepsilon_e \exp\left(-\frac{\ln 2}{25}(x^2+y^2)\right)\,. \tag{2.31}$$

Secondly, we consider

$$\mathbf{U}_2(t=0) = \begin{pmatrix} \rho_0 \\ \varepsilon_v y \exp\left(-\dfrac{\ln 2}{25}(x^2+y^2)\right)\rho_0 \\ -\varepsilon_v x \exp\left(-\dfrac{\ln 2}{25}(x^2+y^2)\right)\rho_0 \\ \dfrac{1}{2}\rho_0(x^2+y^2)\varepsilon_v^2\left(\exp\left(-\dfrac{\ln 2}{25}(x^2+y^2)\right)\right)^2 \end{pmatrix}, \tag{2.32}$$

or

$$\rho' = p' = 0\,, \tag{2.33}$$

$$u' = \varepsilon_v y \exp\left(-\frac{\ln 2}{25}(x^2+y^2)\right)\,, \tag{2.34}$$

$$v' = -\varepsilon_v x \exp\left(-\frac{\ln 2}{25}(x^2+y^2)\right)\,. \tag{2.35}$$

Finally, we consider

$$\mathbf{U}_3(t=0) = \begin{pmatrix} \rho_0 + \varepsilon_a \exp\left(-\dfrac{\ln 2}{9}(x^2+y^2)\right) \\ 0 \\ 0 \\ \dfrac{1-\dfrac{p_0}{\rho_0}}{k-1}\varepsilon_a \exp\left(-\dfrac{\ln 2}{9}(x^2+y^2)\right) \end{pmatrix}, \tag{2.36}$$

or

$$u' = v' = 0\,, \tag{2.37}$$

$$p' = \rho' = \varepsilon_a \exp\left(-\frac{\ln 2}{9}(x^2+y^2)\right)\,. \tag{2.38}$$

3. Finite Element Model

3.1. *Taylor-Galerkin finite element method*

The finite element method has emerged as one of the most powerful methods so far devised. This method has the primary advantages of their computational ease of application to complex geometries, and accurate implementation of differential-type boundary conditions.

These attributes have provided us strong impetus for the utilization of this method in simulating problems in an acoustic environment. When solving a hyperbolic equation, it is plausible to bring in the method of characteristics when conducting spatial discretization. In the finite element context, several variants falling into the characteristic catalog are often referred to, among which they are characteristic finite element method,[7] discontinuous finite element method,[8] and characteristic-Galerkin finite element method.[9] An extensive review of these models was given by Donea.[5] Besides these, a class of Petrov-Galerkin models[10–12] has also gained widespread acceptance, the main difference being the methodology used to introduce the upwinding mechanism into the variational statement. While one model may have a prevailing advantage over another, it is not the subject of the present work. We have restricted ourselves to the Taylor-Galerkin finite element model.

The essence of the Taylor-Galerkin finite element model, proposed firstly by Donea,[13] is exploitation of the Taylor series expansion up to a third-order accuracy in time before performing the Galerkin spatial discretization:

$$F = F^n + \left.\frac{\partial F}{\partial t}\right|^n (t - t_n) + \frac{1}{2}\left.\frac{\partial^2 F}{\partial t^2}\right|^n (t - t_n)^2 + \mathcal{O}((t - t_n)^3)\,, \tag{3.1}$$

$$G = G^n + \left.\frac{\partial G}{\partial t}\right|^n (t - t_n) + \frac{1}{2}\left.\frac{\partial^2 G}{\partial t^2}\right|^n (t - t_n)^2 + \mathcal{O}((t - t_n)^3)\,. \tag{3.2}$$

These procedures are useful in yielding higher accuracy in phase than those underlying either upwind finite difference or other upwinding finite element methods.

3.2. *Fundamental study on the Taylor-Galerkin finite element model*

For the sake of clarity, we begin by considering the following hyperbolic equation in a physical domain D:

$$U_t + F_x + G_y = U_t + AU_x + BU_y = 0\,, \tag{3.3}$$

where A and B represent the characteristic speeds in the x and y directions, respectively.

To develop a time accurate finite element method for hyperbolic problems, consideration is warranted concerning the couplings between the time discretization and the Galerkin spatial approximation. In the hope of attaining a variable upwinding method, we introduce four parameters, α, β, γ, μ, into equations (3.1) and (3.2). In so doing, we have

$$\begin{aligned} F = F^n &+ (t - t_n)\left(\alpha A\frac{\partial U}{\partial t} - \beta A\left(\frac{\partial F}{\partial x} + \frac{\partial G}{\partial y}\right)\right)\Bigg|^n \\ &-\frac{1}{2}(t - t_n)^2\left\{\gamma\left(A^2\frac{\partial^2 U}{\partial t\partial x} + AB\frac{\partial^2 U}{\partial t\partial y}\right)\right. \\ &\left.-\mu\left(A^2\left(\frac{\partial^2 F}{\partial x^2} + \frac{\partial^2 G}{\partial y\partial x}\right) + AB\left(\frac{\partial^2 F}{\partial x\partial y} + \frac{\partial^2 G}{\partial y^2}\right)\right)\right\}\Bigg|^n + \mathcal{O}((t - t_n)^3)\,, \end{aligned} \tag{3.4}$$

$$G = G^n + (t-t_n)\left(\alpha B\frac{\partial U}{\partial t} - \beta B\left(\frac{\partial F}{\partial x}+\frac{\partial G}{\partial y}\right)\right)\Bigg|^n$$
$$-\frac{1}{2}(t-t_n)^2\left\{\gamma\left(BA\frac{\partial^2 U}{\partial t\partial x}+B^2\frac{\partial^2 U}{\partial t\partial y}\right)\right.$$
$$\left.-\mu\left(BA\left(\frac{\partial^2 F}{\partial x^2}+\frac{\partial^2 G}{\partial y\partial x}\right)+B^2\left(\frac{\partial^2 F}{\partial x\partial y}+\frac{\partial^2 G}{\partial y^2}\right)\right)\right\}\Bigg|^n + \mathcal{O}((t-t_n)^3)\,. \quad (3.5)$$

Of the four parameters, they are constrained by $\alpha+\beta=1$ and $\gamma+\mu=1$.

With time derivatives being approximated, one can apply the method of weighted residuals to the remaining ordinary differential equation. Following the same vein as the Galerkin model does in a domain of uniform grid size h, together with the linear basis functions, one can derive the discretized equation. Questions regarding the feasibility of this characteristic model give impetus to conducting a fundamental study. Although the algebra becomes quite tedious, we were led to the following difference equation, written in terms of $\nu_x = A\frac{\Delta t}{\Delta x}$ and $\nu_y = B\frac{\Delta t}{\Delta y}$, taking the delta form for the scalar $\delta U^n (\equiv U^{n+1}-U^n)$:

$$\left[\frac{4}{9}+\frac{2}{9}\gamma(\nu_x^2+\nu_y^2)\right]\delta U^n_{I,J}$$
$$+\left[\frac{1}{9}+\frac{1}{6}\alpha\nu_x-\frac{1}{18}\gamma(2\nu_x^2-\nu_y^2)\right]\delta U^n_{I+1,J}$$
$$+\left[\frac{1}{36}+\frac{1}{24}\alpha(\nu_x+\nu_y)-\frac{1}{36}\gamma(\nu_x^2+3\nu_x\nu_y+\nu_y^2)\right]\delta U^n_{I+1,J+1}$$
$$+\left[\frac{1}{9}+\frac{1}{6}\alpha\nu_y+\frac{1}{18}\gamma(\nu_x^2-2\nu_y^2)\right]\delta U^n_{I,J+1}$$
$$+\left[\frac{1}{36}-\frac{1}{24}\alpha(\nu_x-\nu_y)+\frac{1}{36}\gamma(-\nu_x^2+3\nu_x\nu_y-\nu_y^2)\right]\delta U^n_{I-1,J+1}$$
$$+\left[\frac{1}{9}-\frac{1}{6}\alpha\nu_x-\frac{1}{18}\gamma(2\nu_x^2-\nu_y^2)\right]\delta U^n_{I-1,J}$$
$$+\left[\frac{1}{36}-\frac{1}{24}\alpha(\nu_x+\nu_y)-\frac{1}{36}\gamma(\nu_x^2+3\nu_x\nu_y+\nu_y^2)\right]\delta U^n_{I-1,J-1}$$
$$+\left[\frac{1}{9}-\frac{1}{6}\alpha\nu_y+\frac{1}{18}\gamma(\nu_x^2-2\nu_y^2)\right]\delta U^n_{I,J-1}$$
$$+\left[\frac{1}{36}+\frac{1}{24}\alpha(\nu_x-\nu_y)+\frac{1}{36}\gamma(-\nu_x^2+3\nu_x\nu_y-\nu_y^2)\right]\delta U^n_{I+1,J-1}$$
$$=\left[-\frac{2}{3}\beta(\nu_x^2+\nu_y^2)\right]U^n_{I,J}+\left[-\frac{1}{3}\nu_x+\frac{1}{6}\beta(2\nu_x^2-\nu_y^2)+\frac{1}{3}\mu\nu_x\nu_y^2\right]U^n_{I+1,J}$$
$$+\left[-\frac{1}{12}(\nu_x+\nu_y)+\frac{1}{12}\beta(\nu_x^2+3\nu_x\nu_y+\nu_y^2)-\frac{1}{6}\mu\nu_x\nu_y(\nu_x+\nu_y)\right]U^n_{I+1,J+1}$$

$$+\left[-\frac{1}{3}\nu_y+\frac{1}{6}\beta(-\nu_x^2+2\nu_y^2)+\frac{1}{3}\mu\nu_x^2\nu_y\right]U^n_{I,J+1}$$

$$+\left[\frac{1}{12}(\nu_x-\nu_y)+\frac{1}{12}\beta(\nu_x^2-3\nu_x\nu_y+\nu_y^2)+\frac{1}{6}\mu\nu_x\nu_y(-\nu_x+\nu_y)\right]U^n_{I-1,J+1}$$

$$+\left[\frac{1}{3}\nu_x+\frac{1}{6}\beta(2\nu_x^2-\nu_y^2)-\frac{1}{3}\mu\nu_x\nu_y^2\right]U^n_{I-1,J}$$

$$+\left[\frac{1}{12}(\nu_x+\nu_y)+\frac{1}{12}\beta(\nu_x^2+3\nu_x\nu_y+\nu_y^2)+\frac{1}{6}\mu\nu_x\nu_y(\nu_x+\nu_y)\right]U^n_{I-1,J-1}$$

$$+\left[\frac{1}{3}\nu_y+\frac{1}{6}\beta(-\nu_x^2+2\nu_y^2)-\frac{1}{3}\mu\nu_x^2\nu_y\right]U^n_{I,J-1}$$

$$+\left[\frac{1}{12}(-\nu_x+\nu_y)+\frac{1}{12}\beta(\nu_x^2-3\nu_x\nu_y+\nu_y^2)+\frac{1}{6}\mu\nu_x\nu_y(\nu_x-\nu_y)\right]U^n_{I+1,J-1}\,. \tag{3.6}$$

3.2.1. *Modified equation for the Taylor-Galerkin finite element scheme*

With the grid sizes Δx and Δy being continuously refined, the rate at which the truncation error approaches zero is an important consideration. It is, therefore, reasonable to conduct a modified equation analysis which is rooted in Taylor series expansions. The main reason of conducting this fundamental study comes naturally as a virtue of the modified equation analysis which can provide insights into the dissipation and dispersion properties for the numerical scheme considered. By making use of Taylor series expansion, we can derive the modified equation, in the terminology of Warming and Hyett[14] as follows:

$$\begin{aligned}U_t+AU_x+BU_y=(\alpha+\beta-1)&\left(\frac{1}{2}\nu_x\Delta xAU_{xx}+\nu_x\Delta xBU_{xy}+\frac{1}{2}\nu_y\Delta yBU_{yy}\right)\\&+\frac{1}{12}(2-3\alpha-2\gamma)(\nu_x^2(\Delta x)^2AU_{xxx}+\nu_y^2(\Delta y)^2BU_{yyy})\\&+\frac{1}{12}(-9\alpha-6\gamma-4\mu+6)(\nu_x^2(\Delta x)^2BU_{xxy}+\nu_y^2(\Delta y)^2AU_{xyy})\\&+T_1U_{xxxx}+T_2U_{xxxy}+T_3U_{xxyy}+T_4U_{xyyy}+T_5U_{yyyy}+\cdots,\end{aligned} \tag{3.7}$$

where

$$T_1=\frac{1}{24}A^2\Delta t\Delta x^2[(2\alpha+\beta-2)+\nu_x^2(2\alpha+2\gamma-1)]\,,$$

$$T_2=\frac{1}{6}AB\Delta t\Delta x^2[(\alpha+\beta-1)+\nu_x^2(2\alpha+2\gamma-1)]\,,$$

$$T_3=\frac{1}{12}\frac{\Delta x^2\Delta y^2}{\Delta t}[(\alpha+\beta-1)(\nu_x^2+\nu_y^2)+\nu_x^2\nu_y^2(6\alpha+2\gamma-3)]\,,$$

$$T_4=\frac{1}{6}AB\Delta t\Delta y^2[(\alpha+\beta-1)+\nu_y^2(2\alpha+2\gamma-1)]\,,$$

$$T_5 = \frac{1}{24} B^2 \Delta t \Delta y^2 [(2\alpha + \beta - 2) + \nu_y^2 (2\alpha + 2\gamma - 1)] .$$

Although the algebra to render this modified equation is considerable, it indeed provides a clearer picture of the error distributions both in space and time. To reduce the numerical dissipation error, it is imperative that the coefficients of the leading even-derivative term be zero. This yields

$$\alpha + \beta - 1 = 0 . \tag{3.8a}$$

In a similar manner, we can also eliminate the leading dispersion error by demanding that the coefficients of third-order derivatives U_{xxx} and U_{yyy} be zero. This leads to

$$2 - 3\alpha - 2\gamma = 0 . \tag{3.8b}$$

With the above two equations, it is adequate to preassign the values of control parameters α, β, γ to render a higher-order scheme. Also, $\alpha = \mu = 0$, $\beta = \gamma = 1$ make the rest of the third-order derivatives become zero. The spatial discretizations provided by the present finite element model deserve consideration as viewed from the following modified equation:

$$U_t + AU_x + BU_y = T_1 U_{xxxx} + T_2 U_{xxxy} + T_3 U_{xxyy} + T_4 U_{xyyy} + T_5 U_{yyyy} + \cdots \tag{3.9}$$

Before closing this section, it is worthwhile to point out that the present Taylor-Galerkin approach no more involves any adjustable parameter. In the user's experience, it is common practice to use a Petrov-Galerkin method to maximize accuracy. In the light of higher spatial accuracy presented here, it suffices to say that the underlying prediction scheme shows promise as a tool in predicting the acoustic physics involving hyperbolicity.

3.2.2. *Phase response of the Taylor-Galerkin finite element scheme*

A consistent, stable and convergent high-order scheme does not suffice to acquire acoustic solutions of good quality. In acoustics computations, one is certain of obtaining a prediction error, which manifests itself in the phase error. Generally, a dispersive wave will appear under these circumstances. As a consequence, many current CFD codes fail to retain the inherent nondispersive characteristics even for a much simpler case of uniform mean flow. With this understanding, it is clear that what is of critical importance in acoustics prediction is attributed to its close relation with the phase velocities of all waves supported by the medium governed by the linearized Euler equations. Pursuit of high-order accuracy in phase is thus requisite.

According to Donea *et al.*,[15] it is advantageous to have better phase accuracy by using a finite element scheme underlying the Taylor-Galerkin model, as compared to other finite differences. The retained better phase accuracy is mainly attributable to the inclusion of an extra term in the Taylor series expansion. This eliminates the leading dispersion errors arising from the spatial and temporal discretizations, respectively.

Conducting a phase response analysis amounts to computing the ratio of the semi-discrete phase velocity ϕ_{TG} to the exact phase velocity ϕ_{exact}:

$$r_\phi = \frac{\phi_{TG}}{\phi_{\text{exact}}} .$$

For the target problem (3.3) defined in two dimensions, the exact phase velocities (or frequency), namely $\phi_{\text{exact}} = -(A, B) \cdot (q_x, q_y)$, are obtained directly from the corresponding advection equation:

$$U_{\text{exact}} = U_0 e^{i(q_x x + q_y y + \phi_{\text{exact}} t)},$$

where q_x, q_y denote the wave numbers along x and y direction, respectively.

In a discrete context, characterized by a constant grid spacing $\Delta x = \Delta y = h$, we can normalize the dimensional wave number vector by

$$\boldsymbol{\xi} = (\xi, \eta) = (hq_x, hq_y).$$

Also, to examine how the computed phase velocity varies with the flow direction, we rewrite the velocity vector as a function of advection direction $\theta \equiv \tan^{-1} B/A$:

$$(A, B) = (A^2 + B^2)^{\frac{1}{2}}(\cos\theta, \sin\theta).$$

According to the Von Neumann stability analysis (or Fourier analysis), we can derive the amplification factor G and phase velocity ϕ_{TG} for the proposed scheme given by (3.6):

$$G = \frac{V_1 + V_3 + i(V_2 + V_4)}{V_1 + iV_2} = \text{function}(|\xi|, \theta),$$

$$\phi_{TG} = \tan^{-1}\left(\frac{V_1 V_4 - V_2 V_3}{V_1^2 + V_2^2 + V_1 V_3 + V_2 V_4}\right),$$

where

$$\begin{aligned}
V_1 = {} & \left[\frac{4}{9} + \frac{2}{9}\gamma(\nu_x^2 + \nu_y^2)\right] + \left[\frac{2}{9} - \frac{1}{9}\gamma(2\nu_x^2 - \nu_y^2)\right]\cos\xi \\
& + \left[\frac{1}{18} - \frac{1}{18}\gamma(\nu_x^2 + 3\nu_x\nu_y + \nu_y^2)\right]\cos(\xi + \eta) + \left[\frac{2}{9} + \frac{1}{9}\gamma(\nu_x^2 - 2\nu_y^2)\right]\cos\eta \\
& + \left[\frac{1}{18} + \frac{1}{18}\gamma(-\nu_x^2 + 3\nu_x\nu_y - \nu_y^2)\right]\cos(-\xi + \eta), \\
V_2 = {} & \frac{1}{3}\alpha\nu_x \sin\xi + \frac{1}{12}\alpha(\nu_x + \nu_y)\sin(\xi + \eta) \\
& + \frac{1}{3}\alpha\nu_y \sin\eta + \frac{1}{12}\alpha(-\nu_x + \nu_y)\sin(-\xi + \eta), \\
V_3 = {} & \left[-\frac{2}{3}\beta(\nu_x^2 + \nu_y^2)\right] + \left[\frac{1}{3}\beta(2\nu_x^2 - \nu_y^2)\right]\cos\xi \\
& + \left[\frac{1}{6}\beta(\nu_x^2 + 3\nu_x\nu_y + \nu_y^2)\right]\cos(\xi + \eta) + \left[\frac{1}{3}\beta(-\nu_x^2 + 2\nu_y^2)\right]\cos\eta \\
& + \left[\frac{1}{6}\beta(\nu_x^2 - 3\nu_x\nu_y + \nu_y^2)\right]\cos(-\xi + \eta),
\end{aligned}$$

$$V_4 = \left[-\frac{2}{3}\nu_x + \frac{2}{3}\mu\nu_x\nu_y^2\right]\sin\xi + \left[-\frac{1}{6}(\nu_x+\nu_y) - \frac{1}{3}\mu\nu_x\nu_y(\nu_x+\nu_y)\right]\sin(\xi+\eta)$$
$$+\left[-\frac{2}{3}\nu_y + \frac{2}{3}\mu\nu_x^2\nu_y\right]\sin\eta + \left[-\frac{1}{6}(-\nu_x+\nu_y) + \frac{1}{3}\mu\nu_x\nu_y(-\nu_x+\nu_y)\right]\sin(-\xi+\eta)\,.$$

By virtue of the phase response analysis presented here, it becomes clear that the value of r_ϕ depends both on the wavelength, $\lambda = 2\pi h/|\boldsymbol{\xi}|$, and on the direction of the propagation speed, θ.

For a clear demonstration of the justification for using the present scheme rather than the Lax-Wendroff scheme, we have plotted r_ϕ at different values of the wave length in Fig. 3.1. Noticeable is a significant improvement on the isotropy even at small wavelengths. Pertaining to the better isotropic property, the present finite element scheme can yield fairly accurate solutions irrespective of the flow directions provided that the case considered is that of a reasonly large wavelength.

3.3. *Nonlinear Euler system*

At this point, it remains to extend the aforementioned analysis to wave problems governed by the Euler of Eqs. (2.27) and (2.28). In this study, we consider the following conservation laws which bear a strong resemblance to those of high-speed gas dynamics:

$$\frac{\partial \mathbf{U}}{\partial t} + \frac{\partial \mathbf{F}}{\partial x} + \frac{\partial \mathbf{G}}{\partial y} = \frac{\partial \mathbf{U}}{\partial t} + \tilde{\mathbf{A}}(\mathbf{U})\frac{\partial \mathbf{U}}{\partial x} + \tilde{\mathbf{B}}(\mathbf{U})\frac{\partial \mathbf{U}}{\partial y} = \mathbf{Q} \quad \text{in } \Omega\,, \tag{3.10}$$

$$\mathbf{U}(0, x) = \mathbf{U}_0(x) \quad \text{on } x \in \Omega\,, \tag{3.11}$$

$$\mathbf{U}(t, x) = \mathcal{G}_0(t, x) \quad \text{on } x \in \Gamma\,, \tag{3.12}$$

where

$$\mathbf{U} = [\rho,\ \rho u',\ \rho v',\ \rho e']^{\mathrm{T}}\,, \tag{3.13}$$

$$\mathbf{F} = [\rho u',\ \rho u'^2 + p',\ \rho u'v',\ u'(\rho e' + p')]^{\mathrm{T}}\,, \tag{3.14}$$

$$\mathbf{G} = [\rho v',\ \rho u'v',\ \rho v'^2 + p',\ v'(\rho e' + p')]^{\mathrm{T}}\,, \tag{3.15}$$

$$\mathbf{Q} = [0,\ 0,\ 0,\ -p_0(u_x + u_y)]^{\mathrm{T}}\,, \tag{3.16}$$

$$\tilde{\mathbf{A}} = \begin{bmatrix} 0 & 1 & 0 & 0 \\ \frac{k-1}{2}a^2 - u'^2 & (3-k)u' & -(k-1)v' & (k-1) \\ -u'v' & v' & u' & 0 \\ (k-1)u'a^2 - ku'e' & ke' - \frac{1}{2}(k-1)(a^2+2u'^2) & -(k-1)u'v' & ku' \end{bmatrix}, \tag{3.17}$$

$$\tilde{\mathbf{B}} = \begin{bmatrix} 0 & 0 & 1 & 0 \\ -u'v' & v' & u' & 0 \\ \frac{k-1}{2}a^2 - v'^2 & -(k-1)u' & (3-k)v' & (k-1) \\ (k-1)v'a^2 - kv'e' & -(k-1)u'v' & ke' - \frac{1}{2}(k-1)(a^2+2v'^2) & kv' \end{bmatrix}, \tag{3.18}$$

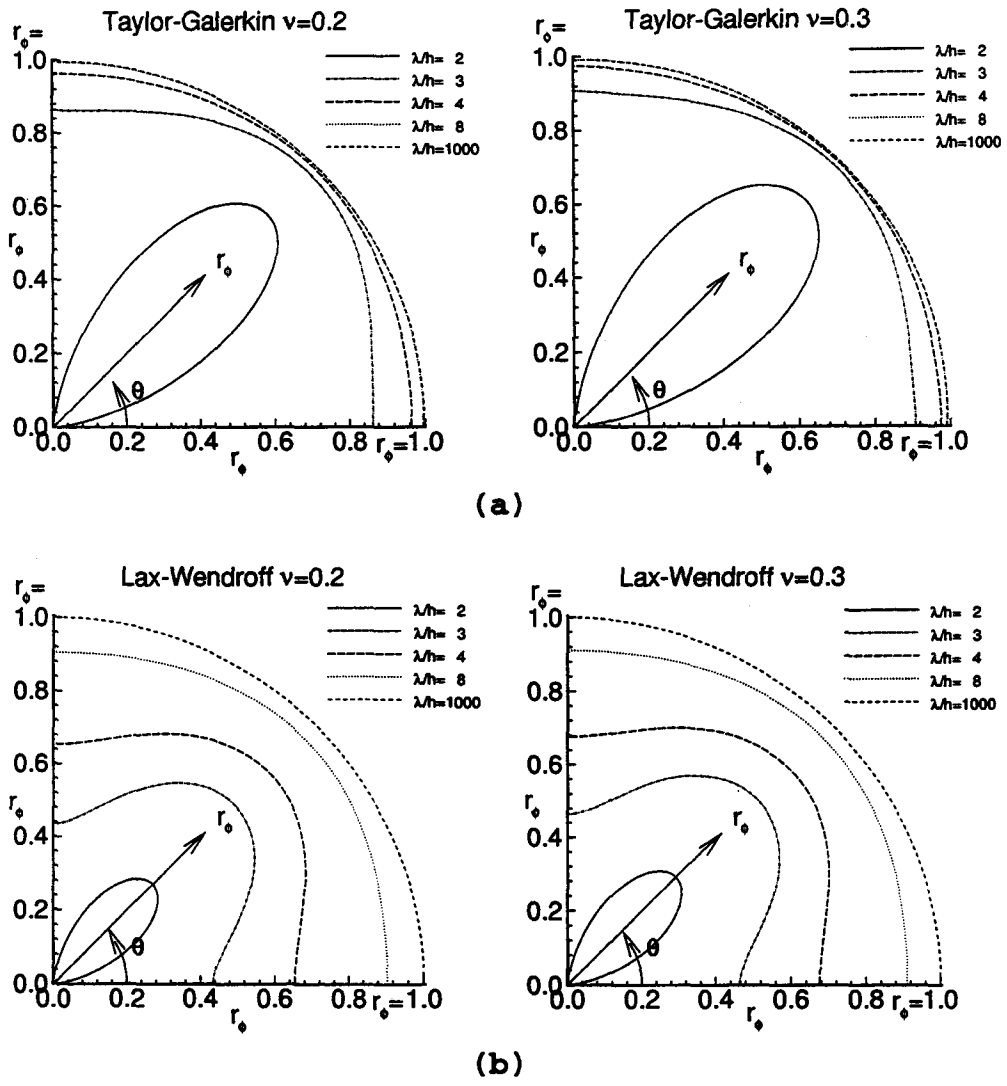

Fig. 3.1. The relative phase velocity r_ϕ against the flow direction θ and normalized wave length λ/h. (a) The present Taylor-Galerkin method; (b) Lax-Wendroff scheme.

$$p' = (k-1)\rho\left(e' - \frac{1}{2}u'^2 - \frac{1}{2}v'^2\right) + \frac{p_0}{\rho_0}\rho'. \tag{3.19}$$

This set of differential equations is classified as the hyperbolic type simply because the Jacobian matrices $\tilde{\mathbf{A}}$ and $\tilde{\mathbf{B}}$ yield real but distinct eigenvalues. The resulting discretized equations capable of representing the change of solution vector between two consecutive time steps can be similarly derived, based on the idea of the Taylor-Galerkin finite element model and on the linear shape functions $N_i = \frac{1}{4}(1+\bar{\xi}_i\bar{\xi})(1+\bar{\eta}_i\bar{\eta})$, where $\bar{\xi}_i$ and $\bar{\eta}_i$ are the normalized coordinates of the ith node.

By referring to $\mathcal{A}$ as an assembly finite element operator, the corresponding discretized equation takes the following form:

$$\mathcal{A}_{el=1}^{n_{el}}([M_{ij}^{el}])\delta\mathbf{U}^n = \mathcal{A}_{el=1}^{n_{el}}([R_i^{el}])\,, \tag{3.20}$$

where

$$R_i^{el} = \sum_j (C_{ij}^{el}\mathbf{F}_J^n + \tilde{C}_{ij}^{el}\mathbf{G}_J^n + S_i^{el})\,, \tag{3.21}$$

$$\begin{aligned} M_{ij}^{el} = \int_{\mathbf{\Omega}^{el}} & \left\{ \mathbf{N}_i\mathbf{N}_j - \frac{1}{2}\alpha\Delta t\left(\frac{\partial \mathbf{N}_i}{\partial x}A + \frac{\partial \mathbf{N}_i}{\partial y}B\right)\mathbf{N}_j \right. \\ & + \frac{1}{6}\gamma\Delta t^2\left[\frac{\partial \mathbf{N}_i}{\partial x}\left(A^2\frac{\partial \mathbf{N}_j}{\partial x} + AB\frac{\partial \mathbf{N}_j}{\partial y}\right) + \frac{\partial \mathbf{N}_i}{\partial y}\left(BA\frac{\partial \mathbf{N}_j}{\partial x} + B^2\frac{\partial \mathbf{N}_j}{\partial y}\right)\right] \Big\} d\mathbf{\Omega}^{el} \\ & - \int_{\mathbf{\Gamma}} \Big\{ -\frac{1}{2}\alpha\Delta t\mathbf{N}_i(n_xA + n_yB)\mathbf{N}_j + \frac{1}{6}\gamma\Delta t^2\mathbf{N}_i\Big[n_x\left(A^2\frac{\partial \mathbf{N}_j}{\partial x} + AB\frac{\partial \mathbf{N}_j}{\partial y}\right) \\ & + n_y\left(BA\frac{\partial \mathbf{N}_j}{\partial x} + B^2\frac{\partial \mathbf{N}_j}{\partial y}\right)\Big]\Big\} d\mathbf{\Gamma}\,, \end{aligned} \tag{3.22}$$

$$\begin{aligned} C_{ij}^{el} = \int_{\mathbf{\Omega}^{el}} & \frac{\partial \mathbf{N}_i}{\partial x}\Big[\Delta t\mathbf{N}_j - \frac{1}{2}\beta\Delta t^2\left(A\frac{\partial \mathbf{N}_j}{\partial x} + B\frac{\partial \mathbf{N}_j}{\partial y}\right) \\ & + \frac{1}{6}\mu\Delta t^3\left(A^2\frac{\partial^2 \mathbf{N}_j}{\partial x^2} + AB\frac{\partial^2 \mathbf{N}_j}{\partial x\partial y} + BA\frac{\partial^2 \mathbf{N}_j}{\partial x\partial y} + B^2\frac{\partial^2 \mathbf{N}_j}{\partial y^2}\right)\Big] d\mathbf{\Omega}^{el} \\ & - \int_{\mathbf{\Gamma}} n_x\mathbf{N}_i\Big[\Delta t\mathbf{N}_j - \frac{1}{2}\beta\Delta t^2\left(A\frac{\partial \mathbf{N}_j}{\partial x} + B\frac{\partial \mathbf{N}_j}{\partial y}\right) \\ & + \frac{1}{6}\mu\Delta t^3\left(A^2\frac{\partial^2 \mathbf{N}_j}{\partial x^2} + AB\frac{\partial^2 \mathbf{N}_j}{\partial x\partial y} + BA\frac{\partial^2 \mathbf{N}_j}{\partial x\partial y} + B^2\frac{\partial^2 \mathbf{N}_j}{\partial y^2}\right)\Big] d\mathbf{\Gamma}\,, \end{aligned} \tag{3.23}$$

$$\begin{aligned} \tilde{C}_{ij}^{el} = \int_{\mathbf{\Omega}^{el}} & \frac{\partial \mathbf{N}_i}{\partial y}\Big[\Delta t\mathbf{N}_j - \frac{1}{2}\beta\Delta t^2\left(A\frac{\partial \mathbf{N}_j}{\partial x} + B\frac{\partial \mathbf{N}_j}{\partial y}\right) \\ & + \frac{1}{6}\mu\Delta t^3\left(A^2\frac{\partial^2 \mathbf{N}_j}{\partial x^2} + AB\frac{\partial^2 \mathbf{N}_j}{\partial x\partial y} + BA\frac{\partial^2 \mathbf{N}_j}{\partial x\partial y} + B^2\frac{\partial^2 \mathbf{N}_j}{\partial y^2}\right)\Big] d\mathbf{\Omega}^{el} \\ & - \int_{\mathbf{\Gamma}} n_y\mathbf{N}_i\Big[\Delta t\mathbf{N}_j - \frac{1}{2}\beta\Delta t^2\left(A\frac{\partial \mathbf{N}_j}{\partial x} + B\frac{\partial \mathbf{N}_j}{\partial y}\right) \\ & + \frac{1}{6}\mu\Delta t^3\left(A^2\frac{\partial^2 \mathbf{N}_j}{\partial x^2} + AB\frac{\partial^2 \mathbf{N}_j}{\partial x\partial y} + BA\frac{\partial^2 \mathbf{N}_j}{\partial x\partial y} + B^2\frac{\partial^2 \mathbf{N}_j}{\partial y^2}\right)\Big] d\mathbf{\Gamma}\,, \end{aligned} \tag{3.24}$$

$$S_i^{el} = \int_{\mathbf{\Omega}^{el}} \Delta t(\mathbf{N}_i\mathbf{Q}_J\mathbf{N}_j)d\mathbf{\Omega}^{el}\,. \tag{3.25}$$

4. Validation Study

Motivated by interests in validating the aforementioned method is of high quality, we consider several benchmark problems. To begin with, we take both linear scalar and nonlinear systems of hyperbolic equations, which are amenable to analytical solutions, into consideration. The computed errors are measured by three norms given below:

$$\|e\|_{L_1(\Omega)} = \int_\Omega |e| dx\,, \tag{4.1}$$

$$\|e\|_{L_2(\Omega)} = \left(\int_\Omega |e|^2 dx\right)^{\frac{1}{2}}\,, \tag{4.2}$$

$$L_\infty = \max_i |e_i|\,, \quad i = 1, 2, \ldots, n\,. \tag{4.3}$$

According to the above definitions, e_i denotes the difference between the finite element solution $\tilde{u}$ and the exact solution u carried out on the basis of n total number of nodes.

4.1. *Two-dimensional linear scalar hyperbolic equation*

As a first model problem, we consider the following equation which corresponds to representing a disturbance, say ρ, propagating constantly in a domain bounded by two ends at $x = \pm 1$ and $y = \pm 1$:

$$\frac{\partial \rho}{\partial t} + A\frac{\partial \rho}{\partial x} + B\frac{\partial \rho}{\partial y} = 0\,. \tag{4.4}$$

This problem serves to demonstrate the effectiveness of the proposed Taylor-Galerkin model. The investigated initial profile of ρ is given by

$$\rho(x, y, t = 0) = \rho(x, y) = \begin{cases} 0; & r > 0.2 \\ 0.25\,\exp[(\ln 2)(r/2)^2]; & r \le 0.2\,. \end{cases} \tag{4.5}$$

Table 1 summarizes the computed error norms defined in (4.1)–(4.3) against different flow directions, namely 0°, 30°, 45°, 60°, and 90°. Also, finite element solutions computed at two uniform mesh sizes enable us to estimate the rates of convergence, as denoted by C in Table 1. The results showing the good agreement with the analytical solution reveal the applicability of the present characteristic-based upwind model to hyperbolic equations.

4.2. *Two-dimensional Euler equations*

To further demonstrate that the underlying finite element model is applicable to a system of hyperbolic equations, the Euler solution $(\rho, \rho u', \rho v', \rho e')^{\mathrm{T}}$ under the influence of a given external source $\mathbf{Q}$ will be presented in the physical domain illustrated in Fig. 4.1.:

$$\mathbf{U}_t + \mathbf{F}_x + \mathbf{G}_y = \mathbf{Q}\,, \tag{4.6}$$

where

$$\mathbf{Q} = \begin{bmatrix} 0 \\ t^2 e^{2t^2} x^2 y + e^{2t^2}(-x^2 y + (k-1)y) \\ t^2 e^{2t^2} x y^2 + e^{2t^2}(-x y^2 + (k-1)x) \\ t e^{2t^2} xy(x^2 + y^2 - 4(k-1)xy) - t^3 e^{2t^2} xy(x^2 + y^2) \end{bmatrix}, \tag{4.7}$$

Table 1. Different error norms for equations (4.4) and (4.5).

$\tan^{-1}\left(\frac{B}{A}\right)$	Mesh size	L_1 norm	C	L_2 norm	C	L_∞ norm	C
0°	10 × 10	2.34213E-03		6.25467E-03		3.02422E-02	
	20 × 20	2.75800E-04	3.08613	7.60573E-04	3.03977	3.18889E-03	3.24544
30°	10 × 10	3.17312E-03		7.41595E-03		3.59134E-02	
	20 × 20	1.59278E-04	4.31628	3.45092E-04	4.42558	1.38936E-03	4.69203
45°	10 × 10	2.89540E-03		7.28986E-03		4.44308E-02	
	20 × 20	2.30603E-04	3.65028	7.50568E-04	3.27984	5.02719E-03	3.14374
60°	10 × 10	3.17312E-03		7.41594E-03		3.59133E-02	
	20 × 20	1.59276E-04	4.3163	3.45090E-04	4.42558	1.38945E-03	4.69193
90°	10 × 10	2.34214E-03		6.25466E-03		3.02422E-02	
	20 × 20	2.75802E-04	3.08612	7.60579E-04	3.03976	3.18930E-03	3.24526

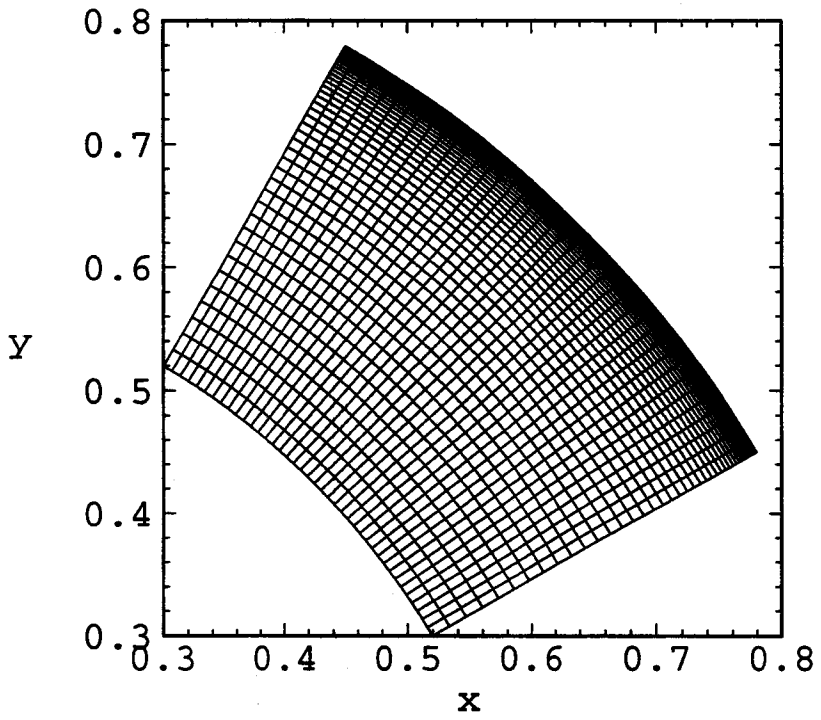

Fig. 4.1. The physical domain and the mesh for the problem discussed in Sec. 4.2.

and

$$p' = (k-1)\rho\left(e' - \frac{1}{2}(u'^2 + v'^2)\right) .$$

The analytic solutions for the above system take the following form:

$$\rho = xye^{2t^2} , \tag{4.8}$$

$$u' = -xt\,, \tag{4.9}$$

$$v' = -yt\,, \tag{4.10}$$

$$e' = 1 + \frac{1}{2}(u'^2 + v'^2)\,, \tag{4.11}$$

$$p' = (k-1)xye^{2t^2}\,. \tag{4.12}$$

Based on the time increment of $\Delta t = 0.0001$, the computed contours on a 40×40 grid system are illustrated in Fig. 4.2, together with the tabulated error-norms for each working

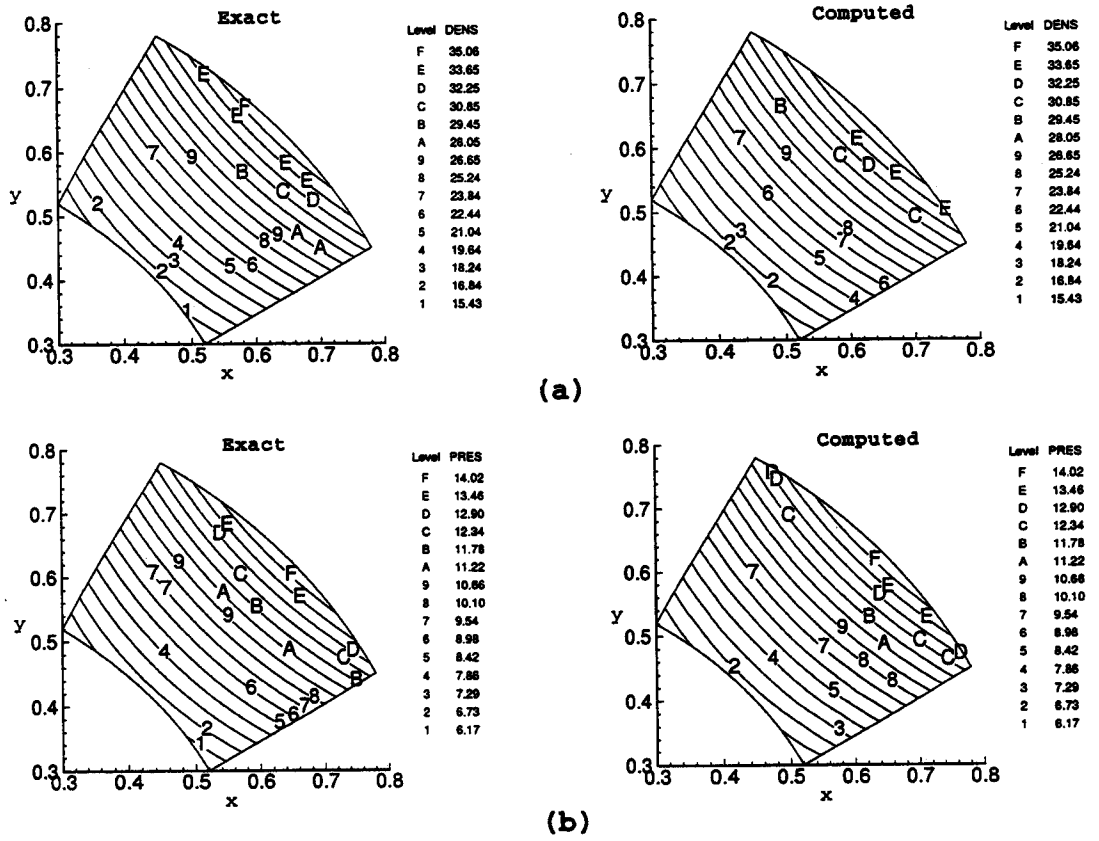

Fig. 4.2. A comparison study for the problem discussed in Sec. 4.2. (a) density contours at $t = 1.5$; (b) pressure contours at $t = 1.5$.

Table 2. The error-norms for the problem discussed in Sec. 4.2.

Variable	ρ	u'	v'	p'
L_1	4.4062E-02	3.5089E-04	3.2810E-04	1.7565E-02
L_2	4.9311E-02	5.6724E-04	4.6781E-04	2.0304E-02
L_∞	0.10313	9.1520E-03	3.0930E-03	6.7260E-02

variable in Table 2. The initial conditions are given according to the equations (4.8)–(4.12) at time $t_1 = 1.4$ while the solutions sought are at time $t_2 = 1.5$.

5. Propagation of Disturbances in a Nonlinear Acoustic System

Having analytically verified the feasibility of the method for Euler equations, we now apply the advective discretization scheme to simulate the transport of disturbances in a nonlinear Euler system. The physical domain of interest is simply taken as a square of length 50 for the acoustic wave while 100 for both entropy and vorticity waves. Regardless of wave modes, 41×41 grid points were uniformly distributed therein. The target problem considered deals with the initial excitations imposed on a quiescent environment. For completeness, three basic waves in a linearized compressible Euler system will be individually considered. This

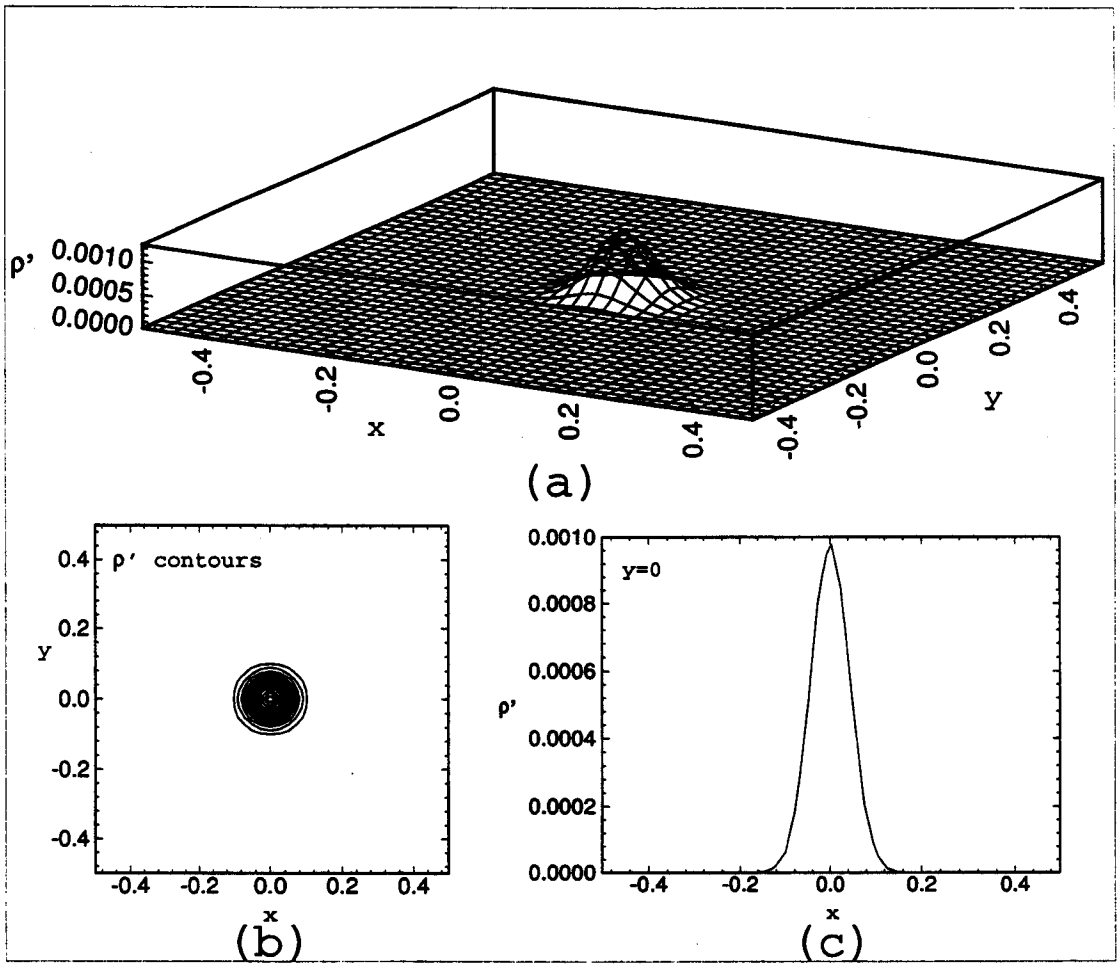

Fig. 5.1. The initial fluctuations of entropy waves. (a) three-dimensional sketch of initial density fluctuation; (b) projection of initial density fluctuation to x-y plane; (c) cross-sectional view of initial density fluctuation at the line $y = 0$.

study is useful in providing analysts with great details about the propagation characteristics because an outgoing disturbance may contain a combination of acoustic, entropy, and vorticity waves. In each simulation, their initial pulse takes a Gaussian profile at the center of the physical domain. The result for each wave at $t = 5$ has been obtained on the basis of $\Delta t = 0.005$.

The main objective of this paper is to discern to what extent a linearized Euler system can be still applied to analysis of acoustic, vorticity, and entropy waves. To achieve this purpose, we conduct the analysis underlying the computer code which relies on the full Euler equations.

5.1. *Numerical simulation of small-amplitude disturbances*

To begin with, we consider disturbances whose amplitudes are regarded as small. We can, thus, compare finite element solutions with those underlying the linearized Euler

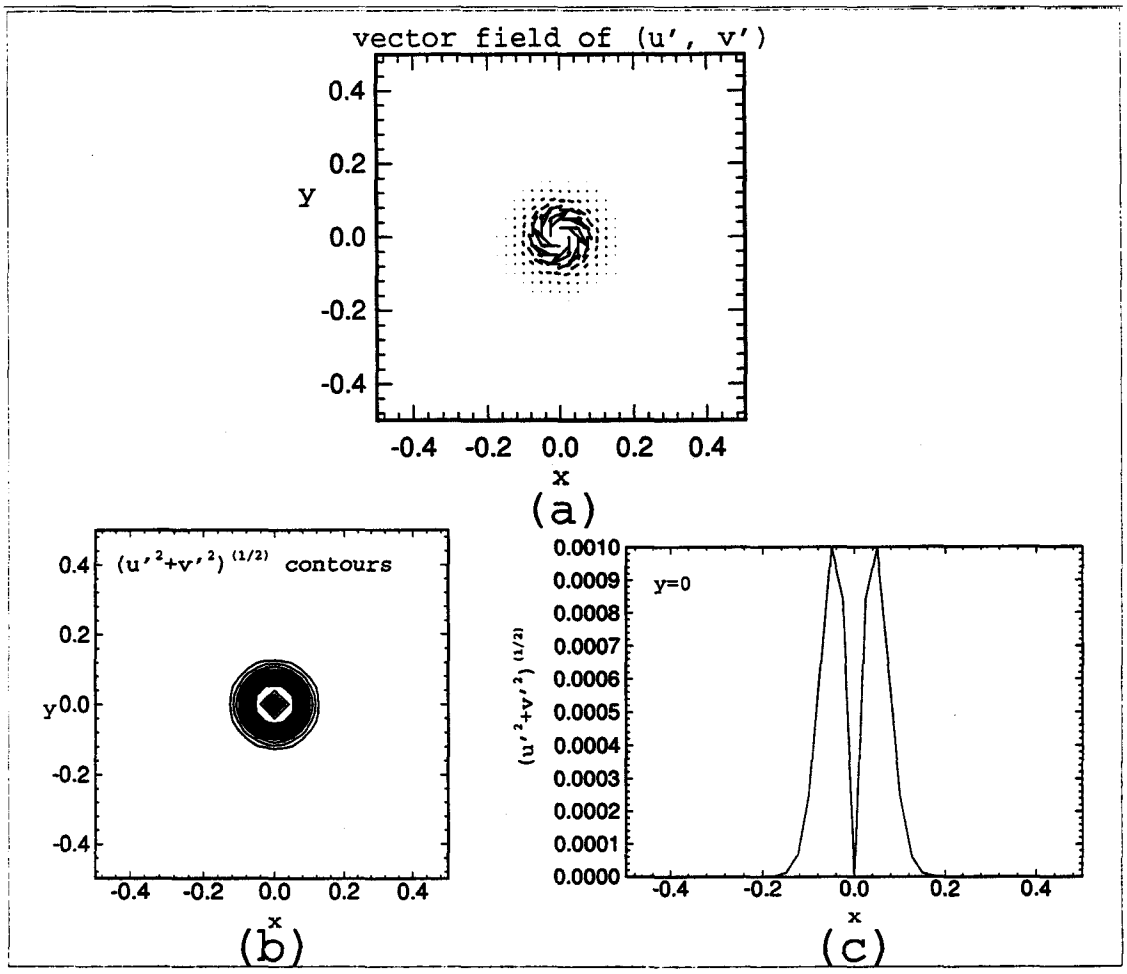

Fig. 5.2. The initial fluctuations of vorticity waves. (a) vector plots of initial velocity fluctuations; (b) contour lines of velocity fluctuations; (c) cross-sectional view of initial velocity fluctuation at the line $y = 0$.

equations (2.1)–(2.4) or the analytic solutions (2.7), (2.8), (2.12)–(2.14) and (2.17)–(2.19). With this objective in mind, the initial conditions investigated are given by equations (2.5), (2.6), (2.9)–(2.11) (2.15) and (2.16), where the pulse amplitudes of entropy, vorticity, and acoustic waves are taken to be $\varepsilon_e = 10^{-3}$, $\varepsilon_v = 4 \times 10^{-4}$, and $\varepsilon_a = 10^{-2}$, respectively. For clarity, we have plotted the initial fluctuations in Figs. 5.1–5.3. Also, the solutions plotted in this section is made against the dimensionless length x/L, and the dimensionless time t/T; where L is the length of square and T is the terminated time.

Subject to the initial conditions given by (2.15) and (2.16), we can predict the ensuing density and pressure waveforms, along the x-axis, in Fig. 5.4. At $t = 5$, both the exact waveforms and those underlying the linearized Euler equations have been plotted for the sake of comparison. Clearly visible is the retained good agreement of three investigated waveforms. Besides these fluctuations, we have also depicted velocity fluctuations, measured

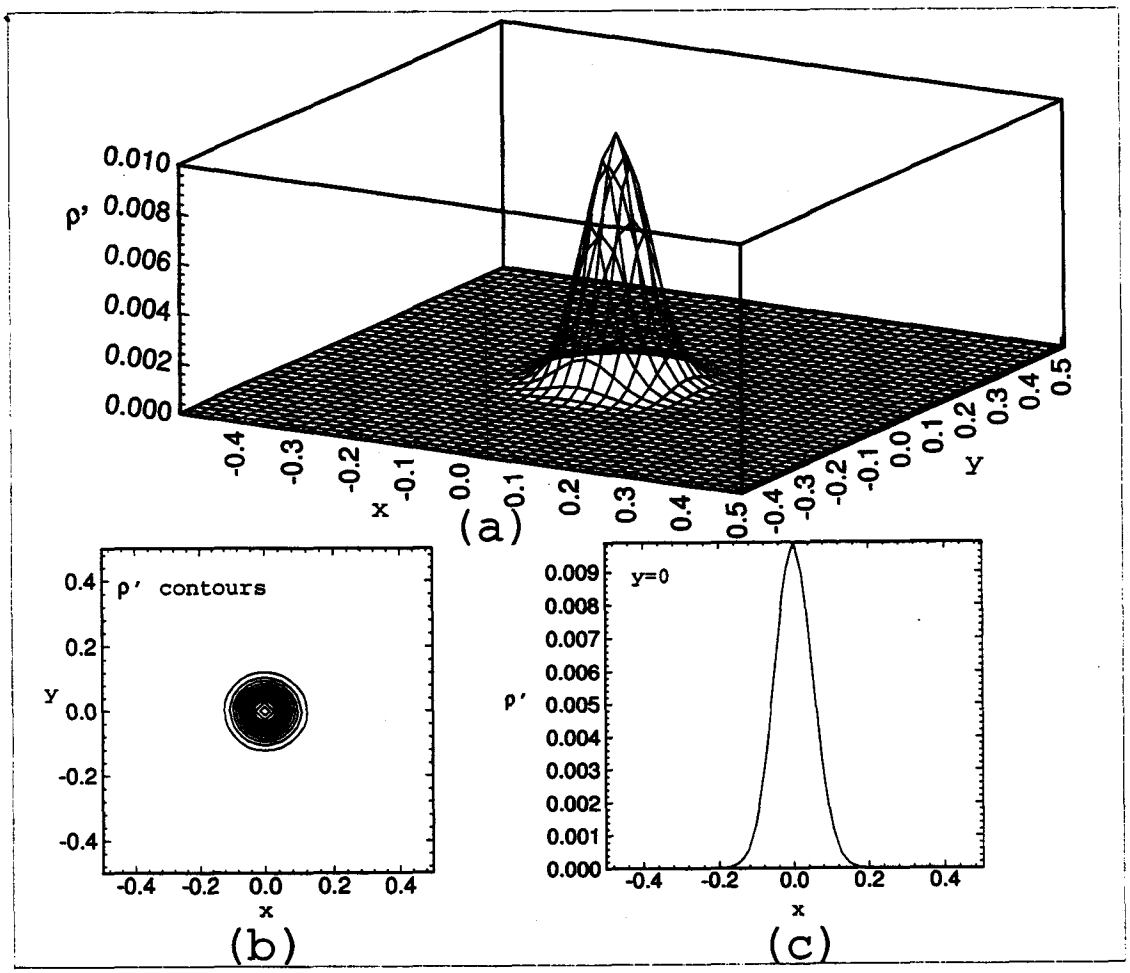

Fig. 5.3. The initial fluctuations of acoustic waves. (a) three-dimensional sketch of initial density fluctuation; (b) projection of initial density fluctuation to x-y plane; (c) cross-sectional view of initial density fluctuation at the line $y = 0$.

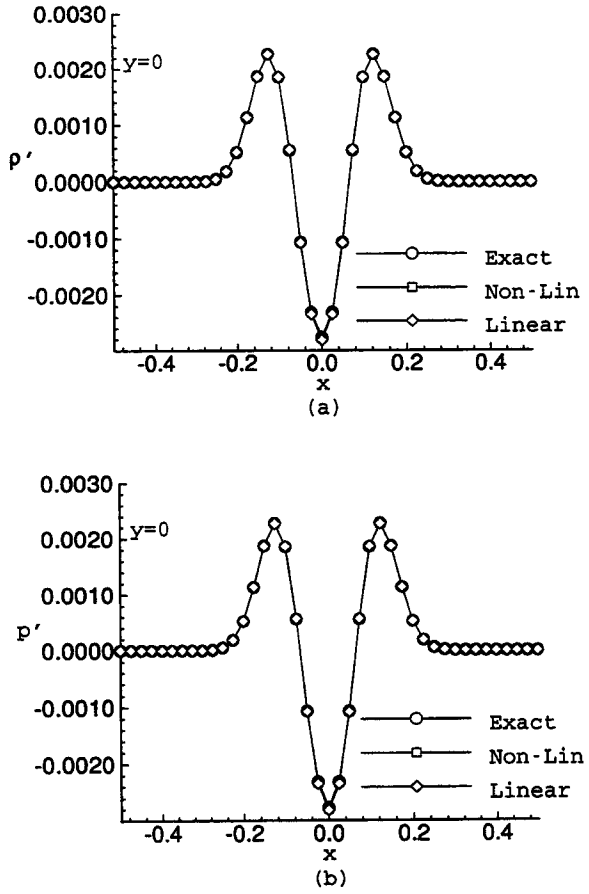

Fig. 5.4. Comparisons of exact fluctuating density and pressure profiles at $t = 5$, with those based on linear and nonlinear Euler equations for the acoustic wave. (a) cross-sectional plot for density fluctuation at $y = 0$; (b) cross-sectional plot for pressure fluctuation at $y = 0$.

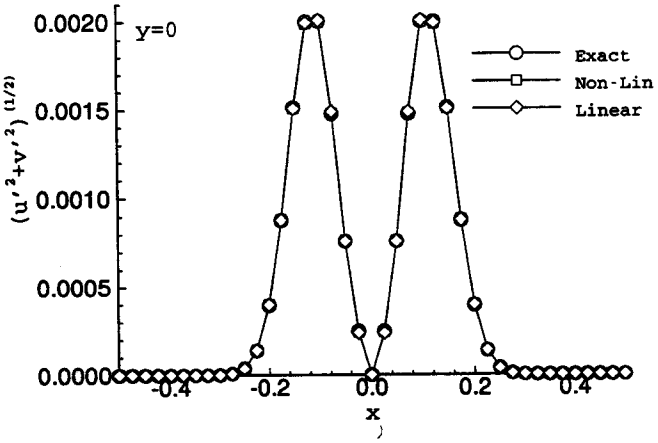

Fig. 5.5. Comparison of exact fluctuating velocity profile at $t = 5$, with those based on linear and nonlinear Euler equations for the acoustic wave.

in terms of $(u'^2 + v'^2)^{\frac{1}{2}}$, in Fig. 5.5, from which we are led to recognize that the scheme considered still performs well in predicting transport of acoustic waves governed by the nonlinear Euler equations. It implies that not only the validity of the computer code but also its applicability to acoustics simulation have been confirmed.

As to the evolutions of entropy and vorticity waves, we have also conducted studies on the basis of the initial conditions of (2.5), (2.6) and (2.9)–(2.11), respectively. Figures 5.6 and 5.7 present the computed nonlinear Euler solutions, together with exact solutions (2.7), (2.8) and (2.12)–(2.14). As convected with the background flow, the entropy waveform is maintained. As a result, the computed stationary solutions are invariant with time. Likewise, there is no visible vorticity variation in the course of wave propagation because it possesses propagation characteristics in common with the entropy wave.

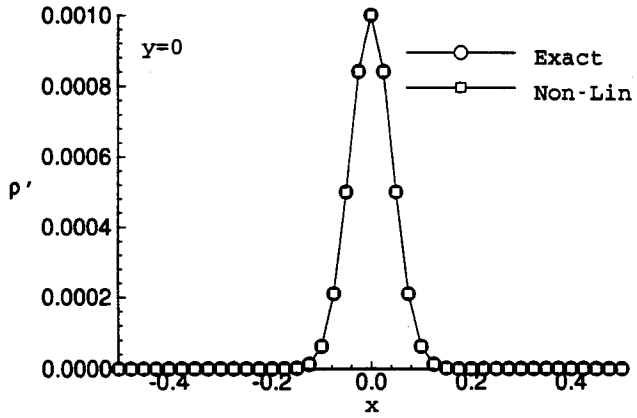

Fig. 5.6. Comparison of exact fluctuating density profile at $t = 5$, with that based on nonlinear Euler equation for the entropy wave.

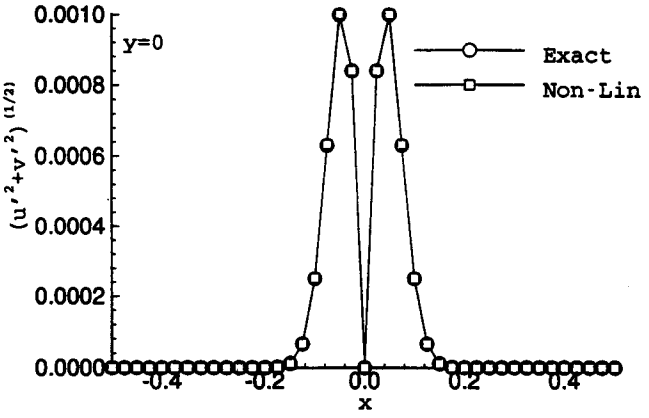

Fig. 5.7. Comparison of exact fluctuating velocity profile at $t = 5$, with that based on nonlinear Euler equation for the vorticity wave.

5.2. *Numerical simulation of large-amplitude disturbances*

We now turn to the investigation of the effect of larger amplitudes on the wave propagation. In view of the fact that the linear Euler equations are no longer appreciable to propagation waves of large amplitudes, to what extent the linear theory is still suitable to simulate three investigated waves is the present concern. To answer this question, we keep increasing amplitudes by 1–10, 20, 30, 40, 50, 100, 500, 1000, 2000, 5000, 10^4 times for acoustic and entropy waves, while 1–10, 20, 30, 40, 50, 100, 500, and 1000 for the vorticity wave.

For ease of illuminating the computed solutions, we have plotted working variables in a dimensionless sense. The solutions for these amplitudes were plotted at $t = 5$ in Figs. 5.8–5.11. Discrepancies from the linear solutions become increasingly apparent with the increase of the amplitudes of the initial wave profiles. It is particularly true for the acoustic wave, followed by the vorticity wave. It is fair to conclude that no change has been observed for the

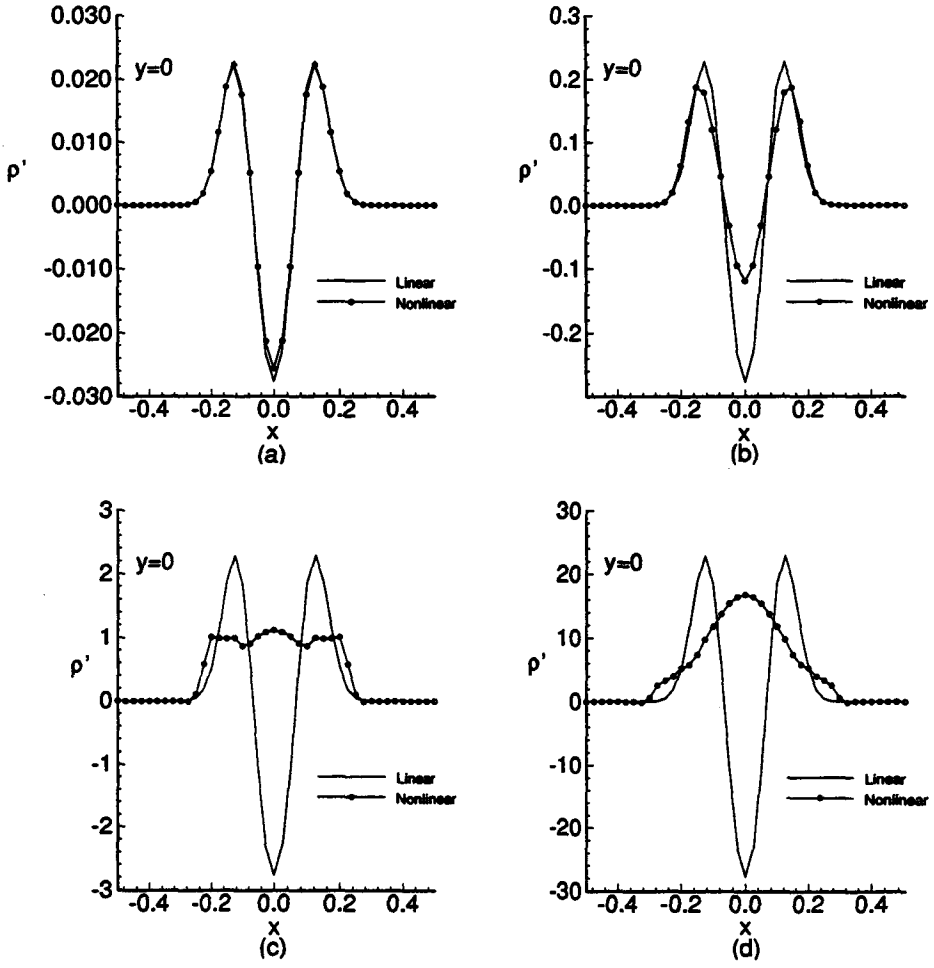

Fig. 5.8. The fluctuating density profiles computed from nonlinear Euler equations for acoustic waves involving different amplitudes. (a) $\varepsilon_a = 10^{-1}$; (b) $\varepsilon_a = 10^0$; (c) $\varepsilon_a = 10^1$; (d) $\varepsilon_a = 10^2$.

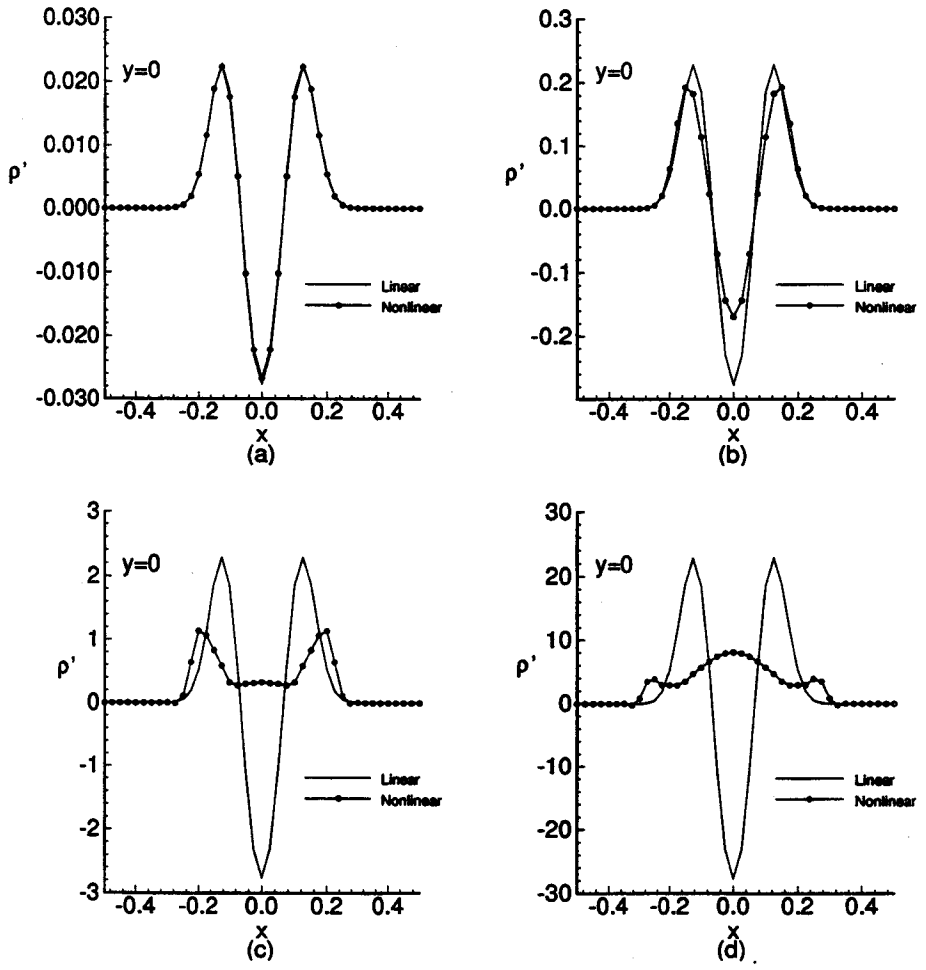

Fig. 5.9. The fluctuating pressure profiles computed from nonlinear Euler equations for acoustic waves involving different amplitudes. (a) $\varepsilon_a = 10^{-1}$; (b) $\varepsilon_a = 10^0$; (c) $\varepsilon_a = 10^1$; (d) $\varepsilon_a = 10^2$.

entropy wave. We distinguish finite element solutions obtained from the full Euler equations from analytic linear solutions in a L_2-norm sense. With an incremental time step $\Delta t = 0.5$, we have presented them against time graphically in Figs. 5.12 and 5.13, for acoustic and vorticity waves, respectively. As to the entropy wave, finite element solutions rendered from linear equations are identical to those based on the nonlinear analyses, regardless of all investigated amplitudes. Also, with the present computed solutions, we are able to know under what circumstances a linear analysis fails to predict the realistic wave propagations. We have summarized them in Fig. 5.14 for the acoustic wave and in Fig. 5.15 for the vorticity wave. The discrepancy from the linear analysis is measured in a percentage sense for the ratio of the L_2-norm of the linear solution and the L_2-norm of predicted difference between the computed nonlinear and linear solutions. For a set of amplitude and time which falls below a contour line, shown in Figs. 5.14 and 5.15, the maximal percentage of the computed

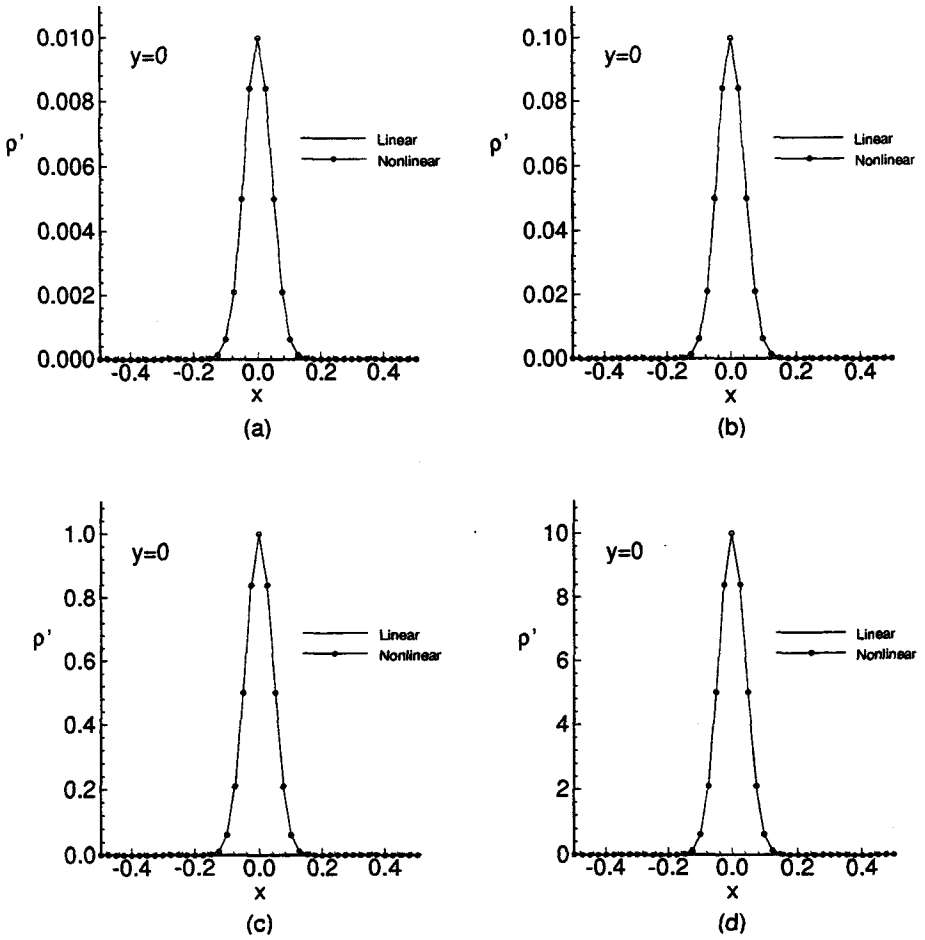

Fig. 5.10. The fluctuating density profiles computed from nonlinear Euler equations for the entropy wave involving different amplitudes. (a) $\varepsilon_e = 10^{-2}$; (b) $\varepsilon_e = 10^{-1}$; (c) $\varepsilon_e = 10^{0}$; (d) $\varepsilon_e = 10^{1}$.

difference between linear and nonlinear solutions fall below the value of this contour line. Among three investigated waves, the computed difference, based on linear and nonlinear analyses, the entropy wave is smaller than the other two waves.

6. Conclusions

1. A generalized framework of the Taylor-Galerkin finite element model has been developed and applied to predict the transport of finite-amplitude disturbances in a two-dimensional domain. Modified equation analysis provides the rule which enables us to assign values to four free parameters *a priori*. This forms the core of the present advection scheme which is characterized as having a third-order spatial accuracy. In the light of the response analysis, the characteristic scheme presented herein furthermore exhibits that a more

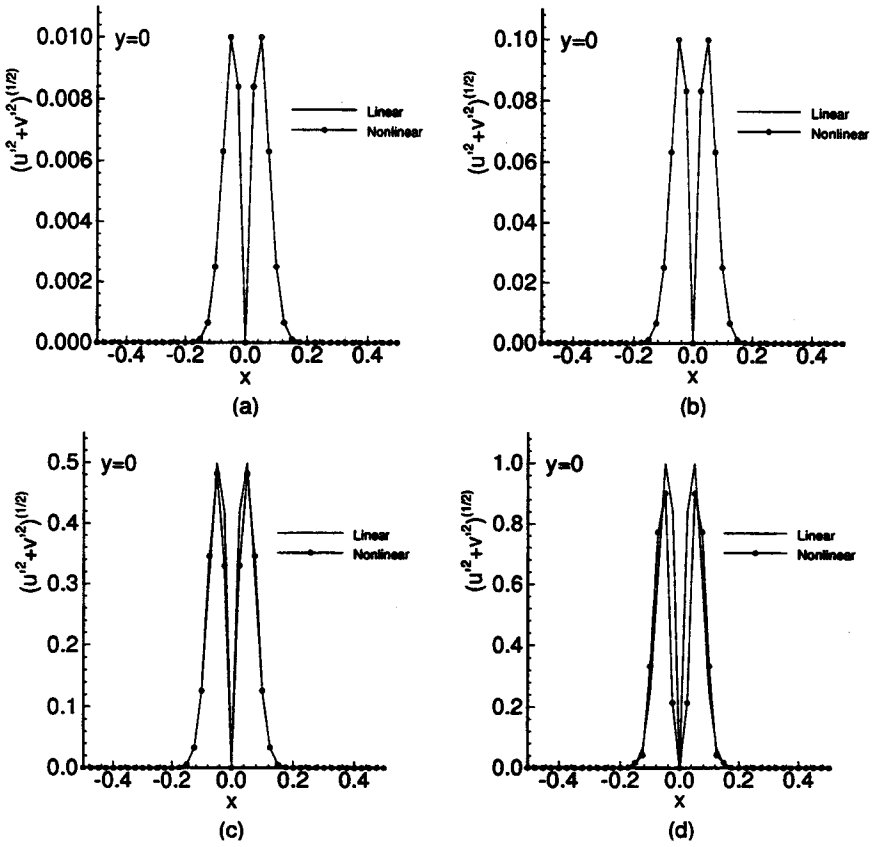

Fig. 5.11. The fluctuating velocity profiles computed from nonlinear Euler equations for the vorticity wave involving different amplitudes. (a) $\varepsilon_v = 4 \times 10^{-3}$; (b) $\varepsilon_v = 4 \times 10^{-2}$; (c) $\varepsilon_v = 2 \times 10^{-1}$; (d) $\varepsilon_v = 4 \times 10^{-1}$.

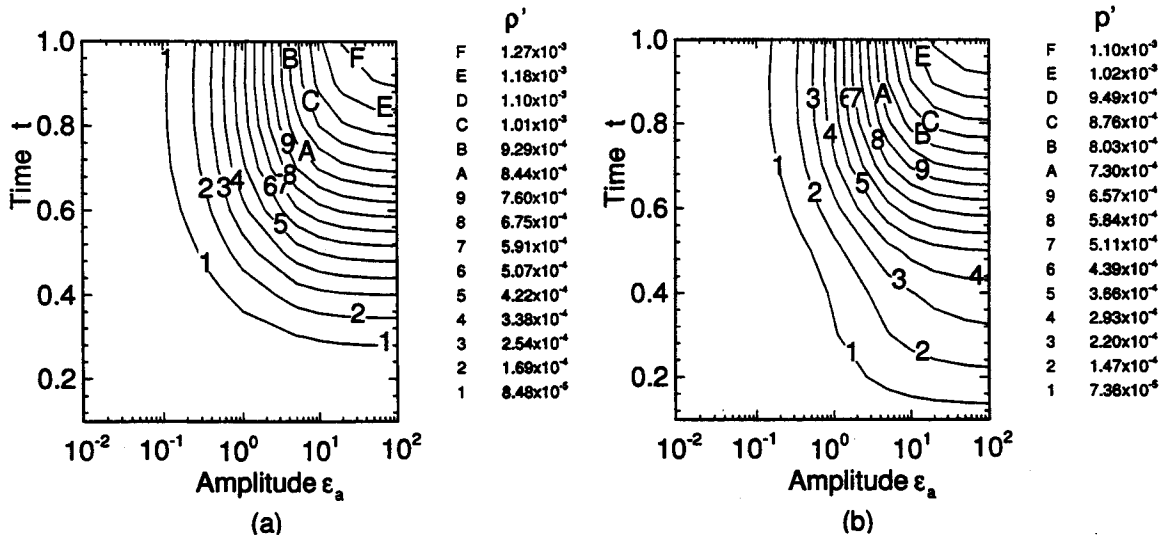

Fig. 5.12. Error norm distributions of density and pressure for the acoustic wave. (a) error contours for density fluctuations; (b) error contours for pressure fluctuations.

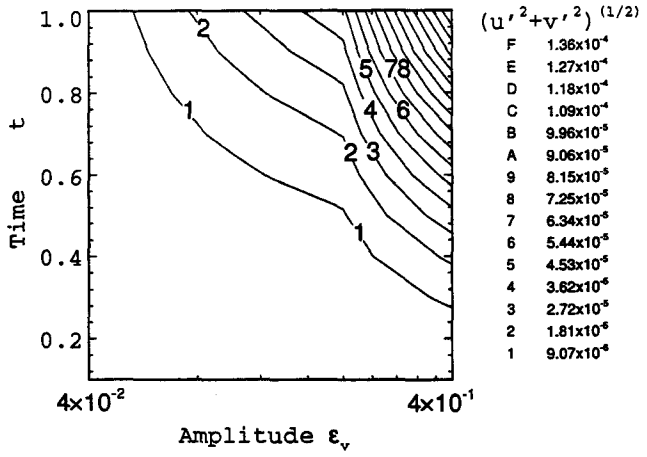

Fig. 5.13. Error norm distribution of velocity for the vorticity wave.

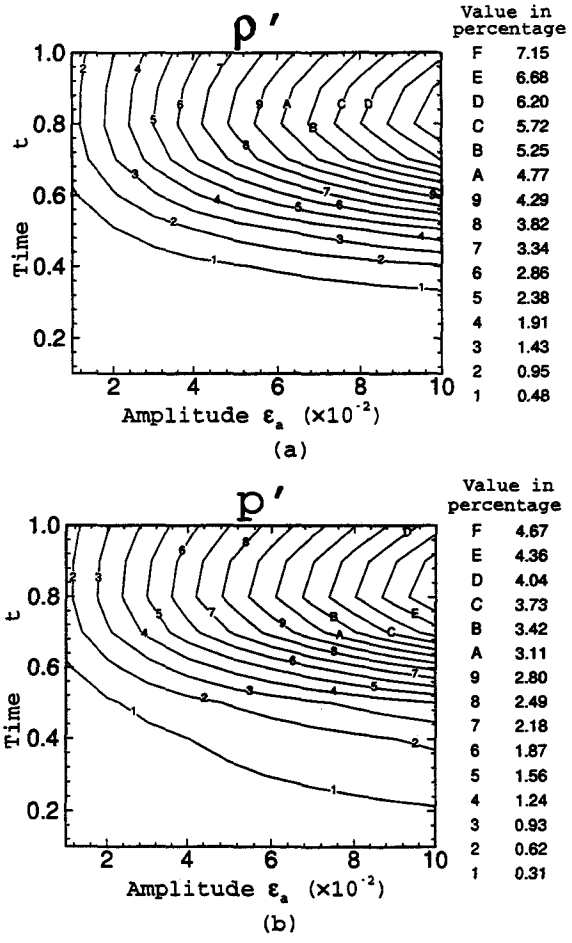

Fig. 5.14. A plot for showing the computed difference between linear and nonlinear analyses. (a) Density in acoustic wave; (b) pressure in acoustic wave.

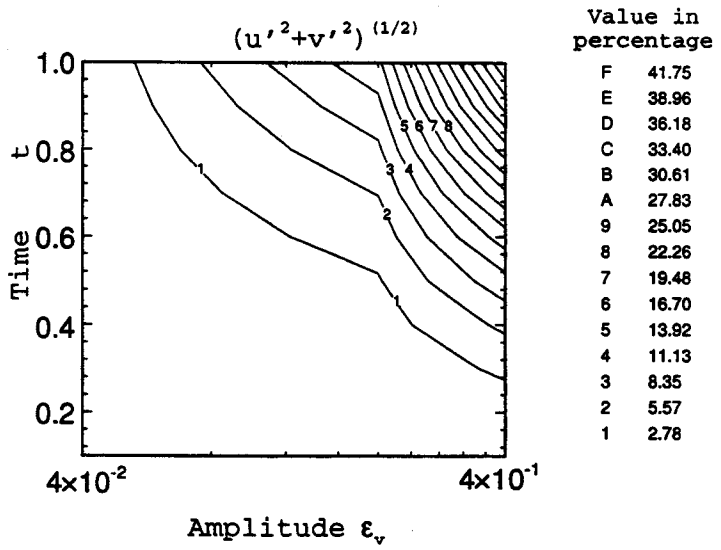

Fig. 5.15. A plot for showing the computed difference between linear and nonlinear analyses. Velocity in vorticity wave.

isotropic character is also attainable. As a vehicle for acoustics simulation, numerical examples amenable to analytical solutions have been presented to confirm the feasibility of the computer code. Good agreement between analytical and computed results has been obtained, either for nonlinear Euler equations or for its degenerated linear scalar transport equation.

2. Thanks to the reduced dispersive, reduced dissipative, and greater isotropic characteristics, numerical simulation of nonlinear propagation of disturbances seems plausible. The underlying assumption made here is that the present analysis is conducted in a quiescent environment. Three initial sets of disturbances, namely entropy, vorticity, and acoustic waves that can be supported in a linearized Euler system, have been studied. The emphasis has been placed on identifying the extent to which the computed solutions are attributable to the nonlinear contributions.

Acknowledgments

The authors would like to thank the Computer Center of National Taiwan University and the National Center for High-performance Computing (NCHC) for providing computers CRAY XMP EA/116se and IBM ES/9000-860 and making this study possible.

References

1. A. D. Pierce, *Acoustics, An Introduction to its Physical Principles and Applications* (McGraw Hill, 1989).
2. J. Glimm, *Comm. Pure Appl. Math.* **18**, 697 (1965).
3. R. Sanders, *Math. Comput.* **40**, 91 (1983).
4. P. D. Lax, *Comm. Pure Appl. Math.* **7**, 159 (1954).

5. J. Donea, *Appl. Mech. Rev.* **44**, 205 (1991).
6. C. K. W. Tam and J. C. Webb, *J. Comput. Phys.* **107**, 262 (1993).
7. K. W. Morton, *Comput. Meths. Appl. Mech. Engin.* **52**, 847 (1985).
8. P. Lesaint and P. A. Raviart, "On a finite element method for solving the neutron transport problem," in *Mathematical Aspects of Finite Elements in Partial Differential Equations*, eds. C. de Boor (Academic Press, 1974), 89–123.
9. J. H. W. Lee, J. Peraire, and O. C. Zienkiewicz, *Comput. Meths. Appl. Mech. Engin.* **61**, 359 (1981).
10. T. J. R. Hughes, M. Mallet, and A. Mizukami, "A new finite element formulation for computational fluid dynamics: II. Beyond SUPG," *Comput. Meths. Appl. Mech. Engin.* **54**, 341 (1986).
11. I. Christie, D. F. Griffiths, A. R. Mitchell and O. C. Zienkiewicz, *Int. J. Num. Meths. Engin.* **10**, 1389 (1976).
12. T. J. R. Hughes, *Int. J. Num. Meths. Engin.* **12**, 1359 (1978).
13. J. Donea, *Int. J. Num. Meths. Engin.* **20**, 101 (1984).
14. R. F. Warming and B. J. Hyett, *J. Comput. Phys.* **14**, 159 (1974).
15. J. Donea, L. Quartapelle, and V. Selmin, *J. Comput. Phys.* **70**, 463 (1981).